surgeries

MDPI

Article

Ionizing Radiation Mediates Dose Dependent Effects Affecting the Healing Kinetics of Wounds Created on Acute and Late Irradiated Skin

Candice Diaz [1,2], Cindy J. Hayward [1,2], Meryem Safoine [1,2], Caroline Paquette [1,2], Josée Langevin [3], Josée Galarneau [3], Valérie Théberge [4], Jean Ruel [5,6], Louis Archambault [6,7,8] and Julie Fradette [1,2,6,*]

1 Centre de Recherche en Organogénèse Expérimentale de l'Université Laval (LOEX), Québec, QC G1J 1Z4, Canada; candice.diaz.1@ulaval.ca (C.D.); cindy.hayward@crchudequebec.ulaval.ca (C.J.H.); meryem.safoine.1@ulaval.ca (M.S.); caroline.paquette.2@ulaval.ca (C.P.)
2 Department of Surgery, Faculty of Medicine, Université Laval, Québec, QC G1V 0A6, Canada
3 Department of Radiation Oncology, Cégep de Sainte-Foy, Québec, QC G1V 1T3, Canada; jlangevin@csfoy.ca (J.L.); jgalarneau@csfoy.ca (J.G.)
4 Department of Radiation Oncology, Centre Hospitalier Universitaire de Québec–Université Laval, Québec, QC G1R 2J6, Canada; valerie.theberge@crchudequebec.ulaval.ca
5 Department of Mechanical Engineering, Faculty of Science and Engineering, Université Laval, Québec, QC G1V 0A6, Canada; jean.ruel@gmc.ulaval.ca
6 Centre de Recherche du CHU de Québec-Université Laval, Québec, QC G1E 6W2, Canada; louis.archambault@phy.ulaval.ca
7 Department of Physics, Université Laval, Québec, QC G1V 0A6, Canada
8 Centre de Recherche sur le Cancer de l'Université Laval, Québec, QC G1R 2J6, Canada
* Correspondence: julie.fradette@chg.ulaval.ca

check for updates

Citation: Diaz, C.; Hayward, C.J; Safoine, M.; Paquette, C.; Langevin, J.; Galarneau, J.; Théberge, V.; Ruel, J.; Archambault, L.; Fradette, J. Ionizing Radiation Mediates Dose Dependent Effects Affecting the Healing Kinetics of Wounds Created on Acute and Late Irradiated Skin. *Surgeries* **2021**, *2*, 35–57. https://doi.org/10.3390/surgeries2010004

Received: 15 December 2020
Accepted: 22 January 2021
Published: 28 January 2021

Publisher's Note: MDPI stays neutral with regard to jurisdictional claims in published maps and institutional affiliations.

Abstract: Radiotherapy for cancer treatment is often associated with skin damage that can lead to incapacitating hard-to-heal wounds. No permanent curative treatment has been identified for radiodermatitis. This study provides a detailed characterization of the dose-dependent impact of ionizing radiation on skin cells (45, 60, or 80 grays). We evaluated both early and late effects on murine dorsal skin with a focus on the healing process after two types of surgical challenge. The irradiated skin showed moderate to severe damage increasing with the dose. Four weeks after irradiation, the epidermis featured increased proliferation status while the dermis was hypovascular with abundant α-SMA intracellular expression. Excisional wounds created on these tissues exhibited delayed global wound closure. To assess potential long-lasting side effects of irradiation, radiodermatitis features were followed until macroscopic healing was notable (over 8 to 22 weeks depending on the dose), at which time incisional wounds were made. Severity scores and biomechanical analyses of the scar tissues revealed that seemingly healed irradiated skin still displayed altered functionality. Our detailed investigation of both the acute and chronic repercussions of radiotherapy on skin healing provides a relevant new in vivo model that will instruct future studies evaluating the efficacy of new treatments for radiodermatitis.

Keywords: radiation; ulcers; skin; wounds; wound healing; radiodermatitis; fibrosis; vascularization; mechanical properties; murine model

1. Introduction

Radiation therapy, in combination with surgery, remains the most effective treatment for the management of many cancers [1,2]. However, skin can be exposed to significant doses of ionizing radiation during the radiotherapy treatment of various solid tumors. Skin toxicity (radiodermatitis) is in fact the most important side effect of radiotherapy [3,4]. More than 85% of patients treated by radiotherapy suffer from moderate to severe skin lesions [4,5]. Patient-related risk factors (e.g., age, microcirculatory pathology, or genetic

disease) as well as technical parameters such as the total dose, the dose fractionation schedule, the site, and the surface area of irradiated tissue have an impact on the incidence and severity of skin reactions [6]. In the most severe cases, radiation can lead to progressive tissue damage ultimately resulting in chronic ulcers [7,8]. These radiation wounds are difficult to heal because of the unpredictable inflammatory episodes that recur weeks or even years after exposure to radiation [9–11]. Radiation-induced fibrosis (RIF) is a complex process at the origin of the recurrence of the lesions and is not fully understood (reviewed in [12]). However, the observed tissue damage is associated with the presence of free radicals and pro-inflammatory mediators such as interleukin (IL)-1β, IL-6, transforming growth factor (TGF)-β1, and connective tissue growth factor (CTGF) [11,13,14]. The skin becomes hypovascular, fibrotic, and hypoxic [15].

Surgical procedures can also accentuate or even reactivate radiodermatitis symptoms. For patients treated for soft tissue sarcoma, surgery can be performed a few weeks after radiotherapy as part of the treatment plan [16]. Similarly, for patients undergoing breast reconstruction after tumor ablation and radiotherapy, surgery is carried out on skin previously exposed to ionizing radiation several months to years after radiation. An important challenge faced by surgeons is the high rate of complications and poor aesthetic results when surgery is performed on irradiated skin. This represents a major issue requiring the establishment of complex and expensive care [17–20]. For example, in the case of preoperative radiotherapy for the treatment of sarcomas, surgery has been reported to be associated with complications in 35% of cases [17]. For post-radiotherapy breast reconstruction, the number of complications and unfavourable results are estimated to be as high as 60% [20]. Irradiation has an extensive and long-lasting impact on the skin healing process and these side effects can be highly debilitating for patients, with possible significant negative impact on their quality of life.

In order to better understand the complications associated with surgical procedures performed on irradiated skin, some studies have used incisional surgery on murine models. The incisional model is considered the most appropriate for evaluating the mechanical properties of scar tissue and for providing indications of the risks of scar rupture [21–25]. On the other hand, the full-thickness excisional wound model is the most representative of deep tumor resection or reconstructive surgery cases, causing defects that extend far into the subcutaneous tissues [26–31]. Excisional models are particularly useful for evaluating new treatments since they provide quantitative data regarding each wound healing phase (e.g., reepithelization, formation of granulation tissue, and neovascularization). Despite the higher contractility and higher hair follicle density of rodent skin in comparison to human skin, murine models can provide important contributions to the study of radiodermatitis and to the testing of novel therapeutics, given that a detailed characterization of each model is performed [32].

To date, there is no permanent curative treatment available for radiodermatitis [33–35]. Standard wound management includes moisturizing creams, hydrogel-based dressings for dry skin, and the use of topical steroids to reduce inflammation [5,35]. These conservative treatments can reduce and alleviate radiodermatitis symptoms, but additional research is needed to identify curative therapies. Promising treatment modalities are emerging, such as the use of oral zinc agents aiming at reducing the emergence of acute signs of radiodermatitis if taken preventively during radiotherapy [36]. A recent case-report study also evaluated the benefit of the topical application of a human fibroblast-derived preparation containing anti-inflammatory cytokines and growth factors for the treatment of a patient with acute radiodermatitis [37]. Other therapies using mesenchymal stem cells (MSCs) are being evaluated for the treatment of irradiated skin in a rodent model [13,38,39], based on the pro-healing effect of their secretome [40–42]. The assessment of the safety and efficacy of new treatments that are being developed requires a better understanding of the negative impact of ionizing radiation on skin cells and wound healing processes. Therefore, our hypothesis is that the impact of ionizing rays will translate into dose-dependent effects on the cells of each compartment of the skin, leading to the impairment

of its healing capacity during both early (acute) and late (chronic) stages of radiodermatitis after radiation. Therefore, three doses of irradiation (45, 60, and 80 Gy) and the progression of radiodermatitis followed over 22 weeks by macroscopic and histological analyses were evaluated in a murine model. To characterize and quantify how the healing process of irradiated skin was impacted, two types of surgical challenge were used: splinted excisional wounds for the analysis of wound closure kinetics on acutely irradiated skin (4 weeks), and incisional wounds on late irradiated skin (8 to 22 weeks). In both models, a significant impairment of the wound healing process was observed. For excisional wounds, delayed global wound closure was observed with a concomitant reduced content of collagen fibers in the granulation tissue. For incisional wounds, even up to 22 weeks after the initial irradiation insult, severity scores and scar rupture assays indicated significant functional alterations of the skin healing mechanisms. Taken together, these results validate that the new murine model we developed adequately recapitulates radiodermatitis features, providing indications of deep and long-lasting damage from the effects of the ionizing radiation on various skin cells.

2. Materials and Methods

2.1. Procurement of Animals and Ethics Approval

Male CD-1 mice (12–13 weeks) were purchased from Charles River Canada (Saint-Constant, QC, Canada) and acclimated before the procedures. The animals were housed in Green Line Tecniplast ventilated cages in a biosafety level 2 room. All mice were maintained in a temperature-controlled room (~23 °C) with 50% humidity (−/+ 5%), a 12/12 hour light/dark cycle, and ad libitum access to food and water. Surgeries and wound healing experiments were performed in dedicated rooms outside of the room where the mice were housed, at the animal facility of the research center of the CRCHU de Québec-Université Laval (Québec, QC, Canada). Animal handling, surgeries, and all other procedures were completed in accordance with the guidelines of the Canadian Council on Animal Care. The personnel of the animal care facility were blinded to the experimental group to which an animal belonged. Protocols (#17-051) were approved by the Comité de Protection des Animaux de l'Université Laval (CPAUL) and Cégep de Sainte-Foy Animal Protection Committees.

2.2. Irradiation Protocol and Experimental Design

The irradiation was performed at the radiation oncology department of Cégep de Sainte-Foy, using a Truebeam medical linear accelerator (linac) (Varian Medical Systems, Palo Alto, CA, USA). The dose distribution was calculated with the treatment planning system (TPS) Eclipse (version 13.5, Varian Medical Systems). The day before irradiation, the animals (16–17 weeks) were shaved on their back and sides. On the day of irradiation, the animals were anesthetized with ketamine (80 mg/kg)—xylazine (8 mg/kg)—acepromazine (1 mg/kg). The anesthesia ensured immobilization during positioning and irradiation. Animals were treated in prone position and immobilized with a plastic half-cylinder to guarantee reproducible positioning. A 1.5 cm bolus was used to place the skin at the point of maximum dose of a 6 MV photon beam. Ultrasound gel (Stevens, Anjou, QC, Canada) was used between the plastic cylinder and the skin of the mouse to avoid air bubbles that would alter the radiation dose distribution. Before the irradiation of each mouse, a three-dimensional image-guided radiotherapy (IGRT) with cone-beam computer tomography (CBCT) was performed to precise the fields localization. An area of 1×1 cm^2 of skin on the upper left dorsal side was irradiated. A single treatment plan was made using the Eclipse treatment planning system (Varian Medical Systems) for each dose level. The dose was delivered with 6 MV photons by tangential beams allowing to limit the irradiation of the internal organs of the animal. Three different doses were delivered: 45, 60, or 80 grays (Gy). Each mouse received only one of these doses, in one fraction. Randomization into groups was mostly guided by the weight of the animals and by the absence of skin abrasions (e.g., shaving burns or scrapes). After irradiation, a tattoo was

made with sterile ink and a 22 g needle to indicate the center of the irradiated area. Finally, atipamezole (1 mg/kg) and saline solution (0.5 mL/kg) were administered subcutaneously. Housing in individual cages started on the day of arrival and was maintained until the end of the experimentation. The schematic of the study experimental design is shown in Figure 1.

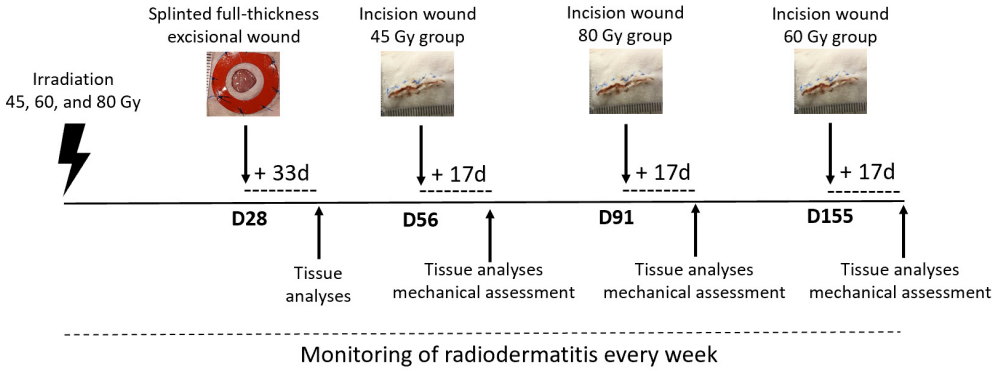

Figure 1. Schematic of the experimental design and timeline of the animal studies. Each week after irradiation, macroscopic images were taken to monitor radiodermatitis progression and resolution. For excisional surgery experiments, two full-thickness excisional wounds were created on the back of CD-1 mice on day 28 after irradiation. Healing was followed visually, and the scar tissues were harvested and processed 33 days later. For the incisional wound study, incisions were made as soon as the skin appeared macroscopically healed for each group, namely on day 56 for the group that received 45 Gy, day 91 for the 80 Gy group, and on day 155 for the group that received 60 Gy (for each time point, a control non-irradiated group was also included). The scar tissues were harvested 17 days after the incisions were made and characterized using mechanical assays.

Two main experiments were carried out with side-by-side comparative experimental groups for each of the three doses (45, 60, and 80 Gy, one experiment for excisional surgery, and one experiment for incisional surgery). Two additional independent experiments were performed for the 0 Gy (control) and 45 Gy groups, as well as for the 0 and 80 Gy groups for excisional surgery studies. The results were analyzed separately, and the results combined when appropriate (thickness measurements), but healing kinetics are reported for side-by-side experiments with the three doses only to avoid potential bias.

2.3. Monitoring of Radiodermatitis Progression

In order to monitor the evolution of radiation-induced skin toxicity over time, macroscopic images were taken every week (once or twice per week) for up to 22 weeks after irradiation. High quality macroscopic images were taken with an EOS Rebel XSi camera (Canon Canada Inc, Mississauga, ON, Canada) positioned on a tripod (Manfrotto 7302YB). During these sessions, the mice were anesthetized with isoflurane and shaved as necessary to ensure good quality images. In order to assess the contribution of skin contraction during the long-term follow-up of mice preceding the incisional study, four tattoo points were made, 21 days after radiation, at the periphery of the irradiated area. The measurement of the proximity of the tattoo points (measurement of the diagonals) was carried out using ImageJ software (ImageJ version 1.51j8, National Institutes of Health, Bethesda, MD, USA, http://imagej.nih.gov/) and compared with the measurement of the distance between the tattoo points on the initial day the tattoo was made (21 day after irradiation). The measurement of the surface area of the erythema (areas delineated by redness) was also made using ImageJ on these macroscopic images. Seven to eight mice per radiation dose were analyzed (one irradiated lesion per mouse).

2.4. Histological Analyses

Tissue samples were harvested and fixed in a 3.7% formaldehyde solution before processing and embedding in paraffin. This was performed at various time-points: on the day of excisional surgery (8 mm punch biopsies at 4 weeks after irradiation), on the final day of analysis (day 33 of healing), as well as on the day of incisional surgery for a subset of two–three mice per time point (see Figure 1 for time points). Sections of 5 µm were made with the microtome (RM2245, Leica, Concord, ON, Canada) and stained with Masson's trichrome or according to a Picrosirius red protocol [43]. Photographs were taken with an AxioCam Icc1 camera mounted on a Zeiss AxioObserver.Z1 microscope (Zeiss Canada, Toronto, ON, Canada) and polarized light was used for viewing the Picrosirius red staining. Scale bars were added to the images using Photoshop (version CC2018, Adobe Systems Inc., San Jose, CA, USA). The thickness of the skin compartments four weeks post-irradiation was measured from these images using ImageJ software for four to sixteen mice per group (one sample per mouse, with five to six measurements per sample). Images were acquired in a semi-blinded manner. At least five to six zones were systematically measured across the whole length of the tissues section to obtain a representative average thickness for each sample. The number of mice analyzed is higher for the 0, 45, and 80 Gy groups since mice from additional independent and comparable experiments were also included. The surface occupied by stained collagen fibers within the entire granulation tissue area visible on Picrosirius-stained transversal sections was quantified using ImageJ for four to five mice per group. The granulation area was identified by the absence of hair follicles and glands on scar tissue.

2.5. Immunolabeling on Tissue Cryosections and Related Analyses

For the excisional wound model, samples of the skin harvested on the day of surgery (4 weeks post-irradiation), and on the day of the final analyses (day 33) were embedded in Tissue-Tek OCT compound (Sakura Finetek, Torrance, CA, USA) and frozen in liquid nitrogen before being stored at −80 °C. Then, 10 µm sections were cut using a cryostat microtome (HM 550, Thermo Scientific, Ottawa, ON, Canada). The samples were permeabilized with acetone before indirect immunofluorescence labeling was performed. The primary antibodies used included rat and rabbit species antibodies directed against the following murine molecules: the endothelial cell marker CD31 (CD31 rat monoclonal, catalog number: 557355, BD Pharmingen, Mississauga, ON, Canada) and α-smooth muscle actin (α-SMA rabbit polyclonal; Ab5694, Abcam, Toronto, ON, Canada) in a co-immunolabeling protocol. The nuclei were stained with 5 mg/mL Hoechst solution (Sigma–Aldrich, Oakville, ON, Canada). Ki-67 staining (Ki-67 rabbit polyclonal Ab15580, Abcam, Toronto, ON, Canada) was also performed. Negative controls consisted of the corresponding isotypic antibodies (rabbit IgG, Ab-105-c, R&D systems, and rat IgG, EMD Millipore, CB2605, Billerica, MA, USA). Detection was carried out using either a goat anti-rat secondary antibody conjugated to Alexa 488 (cat: 1928689, Life technology, Burlington, ON, Canada) or a goat anti-rabbit secondary antibody conjugated to Alexa 594 (catalog number: A-11012, Invitrogen Life, Burlington, ON, Canada). Each antibody was diluted in phosphate-buffered saline (PBS) solution containing 1% (mass/vol) bovine serum albumin (Sigma–Aldrich, Oakville, ON, Canada). Immunofluorescence images were taken with an AxioCam MmR camera mounted on a Zeiss AxioObserver.Z1 microscope (Zeiss Canada, Toronto, ON, Canada). The images were assembled with the stitch function of the software to obtain an image of the entire tissue section. From these images, the analysis of fluorescence was performed using ImageJ software. The detection threshold for the positive signal was set at 49 for CD31 staining and 18 for α-SMA staining (weaker staining). A mean vascular area density was calculated, corresponding to the area of CD31-positive structures per area (mm^2) of the reticular dermis of the skin. The mean density of the α-SMA staining was also calculated, corresponding to the area of α-SMA-positive and CD31-negative structures (to discriminate pericytes) per area (mm^2) of the papillary dermis of the skin. Three to five randomly selected mice per group were evaluated,

using two distinct cryosections per mouse (one wound per mouse). The quantification of the Ki67-positive structures in the epidermis (basal and suprabasal layers) was performed using the Cell Counter plugin of the ImageJ software. The percentage corresponds to the number of positive cells over the total number of cells present (determined by Hoechst staining) per imaging field. Two to six randomly selected mice per group were evaluated, using two distinct cryosections per sample (one wound per mouse), and two large fields per sample.

2.6. Surgical Procedures on Animals

All animal manipulations were performed under isoflurane anesthesia. During the preoperative period, the following analgesics were given: buprenorphine (0.05 mg/kg) and followed by a mixture of lidocaine (7 mg/kg) and bupivacaine (3.5 mg/kg) injected subcutaneously. Post-operatively, carprofen (20 mg/kg), saline solution (1.5 mL), and ceftazidime (30 mg/kg) were administered subcutaneously over 7 days. The skin of the back was delicately shaved and disinfected with a gauze soaked in a mixture of chlorhexidine and alcohol. The following two types of surgeries were performed:

Excisional splinted wounds: Four weeks after irradiation (acute stage radiodermatitis), two full-thickness wounds per mice were created on their mid-back using 8 mm diameter biopsy punches (Acuderm Inc., Fort Lauderdale, FL, USA). One wound was created on the left flank at the site of the initial tattoo located in the center of the irradiated area. The other wound created on the right flank in non-irradiated skin acted as an internal control. Data from these wounds are not presented here. Data from control mice were compiled only from non-irradiated mice (left and right flanks) to prevent a potential bias from any systemic impact of radiation. The panniculus carnosus covering the bared muscle was removed. The 8 mm biopsies were carefully preserved for histological analyses of irradiated and healthy skin. Silicone rings were then centered around the wound margins, fixed with surgical glue (VETBOND™, 3M, London, ON, Canada) and secured with eight monofilament Prolene sutures 5-0 (Ethicon, Johnson & Johnson Medical, Markham, ON, Canada). The use of silicone rings considerably reduces the contraction component that is a major healing mechanism in rodents, thus allowing to better mimic of wound healing processes in humans [28]. As in our previous work [29], the wound was protected (moist wound healing) by coverage with a Mepitel silicone mesh (Mölnlycke Health Care, Oakville, ON, Canada) to which Intrasite gel (Applipak 0.1 mL, Smith&Nephew, Mississauga, ON, Canada) was applied. A Tegaderm™ transparent film tissue adhesive (3M, London, ON, Canada) trimmed to fit each mouse was then laid down to cover both wounds. Mice were finally wrapped in a small layer of cohesive bandage (AMD Ritmed, Lachine, QC, Canada). The wound healing was monitored by macroscopic imaging on the day of surgery and every week afterwards for 33 days (day of terminal analyses), in order to establish healing kinetics for three to four animals per group (two wounds per mouse). On the final day, the mice were euthanized, and scar tissues were harvested for histological analyses.

Incisions: As soon as the skin appeared macroscopically healed (at a different time for each radiation dose, Figure 1), full-depth incisional wounds of 2.5 cm in length were made in the irradiated area (left flank), as well as in the contralateral healthy skin (right flank: control and internal reference). This longitudinal incision corresponded to a median line going in the direction of the lower back of the mouse and was made with Iris scissors. The margins of the wounds were immediately closed with six mattress-type sutures (monofilament 5-0 Prolene, Ethicon, Johnson & Johnson Medical, Markham, ON, Canada). On day 10, any remaining sutures were removed delicately. Wound healing was monitored by taking macroscopic images every 2–3 days over 17 days after surgery (day of terminal analyses), at which time the mice were euthanized, and scar tissue harvested. Mechanical assays were performed for four to six mice per irradiation group (one wound per mouse), and two to three mice for the control group (two wounds per mouse). The contralateral right sides of irradiated mice (left side) did not show any difference with the control group,

so these values were combined with the incision control group (in total eight to ten control wounds) for the mechanical analyses.

2.7. Macroscopic Imaging of the Wounds for Measurements and Scoring Analyses

In order to monitor the healing of wounds, macroscopic images were taken once per week for excisional wounds and three times per week for incisional wounds. The mice were anesthetized with isoflurane and shaved (if necessary) to ensure good quality images. For excisional wounds, global open wound areas were measured using ImageJ. Global wound closure (%) was calculated using the open wound area at a given day relative to the wound area measured on the day of surgery (day of reference). For incisional wounds, qualitative analyses of the appearance of the incisional scarring on the left flank was performed by two evaluators and a mean score was calculated from data acquired from six mice per irradiation group, and seven mice for the control group (one wound per mouse). Three criteria were assessed: redness/inflammation; contraction/waviness of the incision; lack of union/cohesion of the wound margins. Scores ranged from 0 to 3 for each criterion, with 3 indicating the highest severity. In addition, the day on which the scab fell was determined, as well as the number of days elapsed until complete macroscopic healing was observed.

2.8. Evaluation of the Mechanical Properties of Skin after Incisional Surgery

Seventeen days after the incisional wounds were created, ex vivo uniaxial tensile tests were performed in order to evaluate the mechanical properties of the incisional scar tissue, as well as of intact non-wounded skin for comparison. The engineer performing the mechanical test assays was blinded to the experimental group to which an animal belonged. The underlying muscle was removed from the biopsy in order to measure skin properties only. The sample was cut into a bone shape with a custom-made punch, making sure that the skin to be tested was located in the central and thinner section (2 mm width) of the bone-shaped specimen. The extremities of each sample were clamped to a tensile tester (Instron E1000, Instron Corp, Norwood, MA) and each specimen was stretched at a rate of 0.2 mm/s until failure. The $\pm$10 N load cell (Instron 2530-10 N) was used. Two mechanical properties were evaluated: the ultimate tensile strength (UTS, in MPa) corresponding to the breaking strength of the specimen divided by its cross-section (thickness multiplied by the width of the sample measured before tensile testing) in the central portion, and the modulus of elasticity (MPa) consisting of the slope of the stress–strain curve in its linear region. The measurement of the thickness of the scar tissue was made on histological sections stained with Masson's trichrome from biopsies taken near the site where the skin used for mechanical testing was harvested. In total, five to six mice per group (five to six wounds) and two to three mice for the control group per time point (four to six wounds) were evaluated. Since values for the contralateral right sides of the mice (five to six mice) irradiated on the left flank were not significantly different from the values obtained for the non-irradiated control group (five to six wounds, values in blue for the non-irradiated group), they were combined and the average is reported for the incision control group. In addition, measurements of the mechanical properties of intact non-wounded skin from non-irradiated mice of the same age were made, which allowed us to express the results as a percentage of functional recovery of the incisional scar tissue compared to intact non-wounded skin.

2.9. Statistical Analyses

Statistics are presented as mean $\pm$ standard deviation (SD). Statistical analyses were performed using GraphPad Prism 8 software (GraphPad Software Inc., San Diego, CA, USA) and the details are specified in each figure's caption. The confidence interval was set at 95% ($p < 0.05$).

3. Results

3.1. Skin Toxicity Evolves over Time and Is Dose Dependent

Radiation doses of 20 or 30 Gy did not result in visible skin damage at the macroscopic or histological levels four weeks after irradiation (data not shown). However, the impact of increasing radiation doses (45, 60, and 80 Gy) was evaluated over several weeks by documenting radiodermatitis progression weekly using high quality images (Figure 2A). Skin desquamation and alopecia of the irradiated areas were clearly visible 14 days after irradiation for the three doses studied. Large areas of erythema were visible as soon as day 14 for the 80 Gy dose. Animals developed skin damage of variable intensity even within the same experimental group, as shown for the 80 Gy dose (Figure S1). The surface area affected by erythema varied over time and was maximal 21 days post-irradiation for all doses, covering 141.8 $mm^2 \pm 51.9$ for the 80 Gy dose, 140.8 $mm^2 \pm 33.7$ for the 60 Gy dose, and 95.6 $mm^2 \pm 61.9$ for the 45 Gy dose (Figure 2B). Then, the extent and intensity of redness gradually diminished alongside noticeably increased skin contraction, especially for the 80 Gy and 60 Gy groups. Indeed, for a subset of animals, contraction was assessed by measuring the proximity of diagonally opposed tattoo points located at the periphery of the irradiated area (visible in Figure 2A). A contraction peak of 12.8% was observed for the dose of 80 Gy on day 49 after irradiation, while the peak of contraction (10.2%) for the 60 Gy group was observed on day 91. Only limited contraction of 2.3% was observed for the 45 Gy group, peaking on day 49 after radiation. The monitoring of radiodermatitis indicated a wide range of skin toxicity among the animals of each experimental group (Figure 2B). The resorption of redness and desquamation was usually gradual and led to a state of "macroscopic healing" defined as the absence of redness and of visible scarring by visual assessment. Using this definition, on day 56, 86% of the mice of the 45 Gy group were considered asymptomatic in comparison to 14% for the 60 Gy dose, while all mice from the 80 Gy group still exhibited signs of skin toxicity (Table 1). One mouse in the 45 Gy group described as asymptomatic at day 42, showed reactivation of redness at day 56. For the mice that received the 60 Gy dose, radiodermatitis resorption was also gradual, with 86% of the mice categorized as asymptomatic by day 155. One mouse evaluated as asymptomatic on day 91 showed signs of radiodermatitis reactivation on day 113. For the group that received the dose of 80 Gy, a small residual scar was typically visible at day 70, which did not evolve any further with time. This state of stagnation and small residual redness were observed for all but 25% of the mice on day 91, indicating deep cutaneous damage impeding complete further skin regeneration. In comparison, macroscopic healing was observed for 29% of the mice in the 60 Gy group on day 91, but scar resorption continued until day 155 for this group (Table 1).

In order to fully characterize the impact of irradiation on skin cells, we selected two surgical wound healing models, each providing relevant information on the degree of healing impairment resulting from the irradiation. First, acute effects were studied following the creation of excisional wounds in the irradiated area 28 days after irradiation. Then, in order to assess the healing capacity of the irradiated skin at later times, in a late or chronic setting, a simpler incisional wound model was used on macroscopically healed skin (45 and 60 Gy groups), or when the skin damage did not evolve anymore (80 Gy group), which occurred at the time-points indicated in Figure 2A for each radiation dose (red arrows).

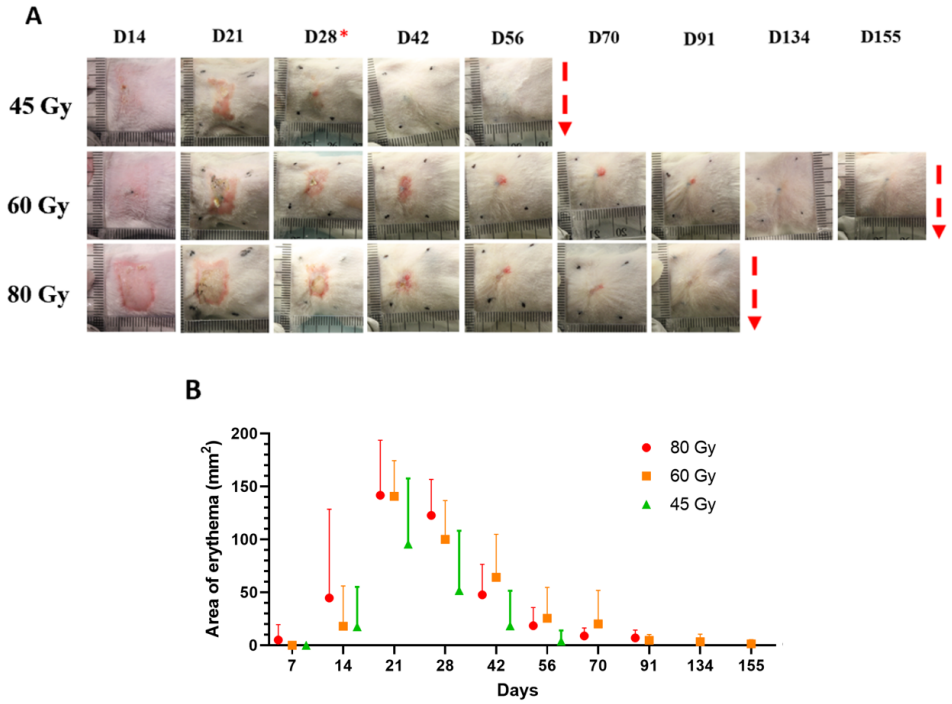

Figure 2. Macroscopic imaging following irradiation and scoring of acute/late side effects. (**A**) Representative images of the appearance of the skin as function of the irradiation dose delivered. * Indicates the date of surgery for excisional wounds created in the irradiated zones and normal skin. Red arrows indicate the day of surgery for incisional wounds. (**B**) Graphical representation of the skin surface area presenting redness over a 22-week period (mean data and standard deviation for n = 7–8 mice per group).

Table 1. Number of mice presenting visually asymptomatic skin at specified time points.

Dose	Day 56	Day 91	Day 155
45 Gy	6/7 (86%)	NA	NA
60 Gy	1/7 (14%)	2/7 (29%)	6/7 (86%)
80 Gy	0/8 (0%)	2/8 (25%) *	NA

NA: not available. * The remainder of the mice presented very small but persistent signs of skin damage that stagnated, and therefore were not compiled as visually asymptomatic.

3.2. Acute Effects: Epidermal Thickness and Proliferative Status Are Increased in Murine Irradiated Epidermis 28 Days after Irradiation

Acute effects typically occur within weeks after radiation, since radiodermatitis features appear and are maintained during the first few weeks after the initial radiation. They include redness, alopecia, and desquamation of the skin. Therefore, the impact of increasing radiation doses was analyzed on the three skin compartments 28 days after irradiation. First, epidermal changes were evaluated (Figures 3 and 4). The thickness of the epidermis was measured on the histological sections stained with Masson's trichrome (Figure 3, purple cell layer). The mean epidermal thickness of normal skin (14.9 ± 3.2 µm) was significantly increased following irradiation at doses of 45 Gy (85.5 ± 27.7 µm), 60 Gy (133.2 ± 12.7 µm), and 80 Gy (129.3 ± 15.5 µm) (Figure 4A). For the 60 and 80 Gy doses, hyperkeratosis was also observed in some areas featuring an abundant stratum corneum (Figure 3). The noticeable increase in epidermal thickness at day 28 post-irradiation was associated with an enlargement of the hair follicle outer root sheath layers, as well as an increase in the epidermal proliferative status as shown by Ki-67 cell labeling (Figure 4B,C). The number of Ki-67 positive nuclei was increased 5-fold in the epidermis of irradiated skin compared to the epidermis of normal skin (Figure 4C). However, for the higher doses of irradiation, living epidermis was not systematically present at day 28 post-irradiation.

In fact, 50% of the samples processed as cryosections partially lacked an epidermis for the 60 Gy dose, while for the 80 Gy dose, 40% of the samples lacked an epidermis or displayed non-cohesive zones of neoepidermis, indicative of extensive tissue damage.

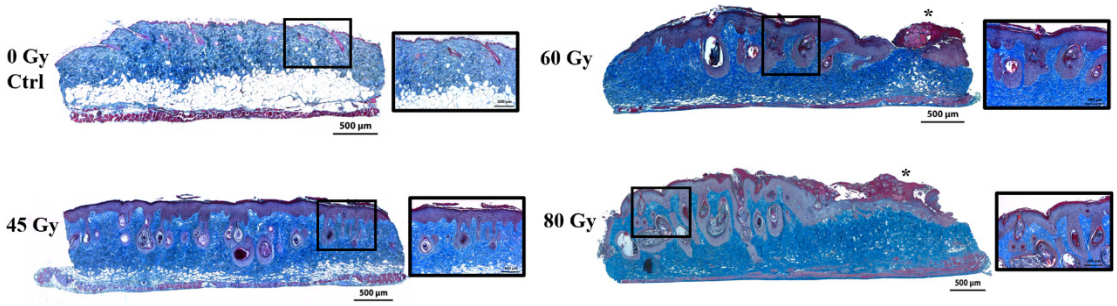

Figure 3. Impact of increasing doses of radiation on the histological appearance of murine skin. Masson's trichrome staining of transverse sections of non-irradiated and irradiated skin 28 days after irradiation. Bars = 500 µm. Images on the right are magnifications of the area delimited by the black boxes. Bars = 200 µm. * indicates hyperkeratosis.

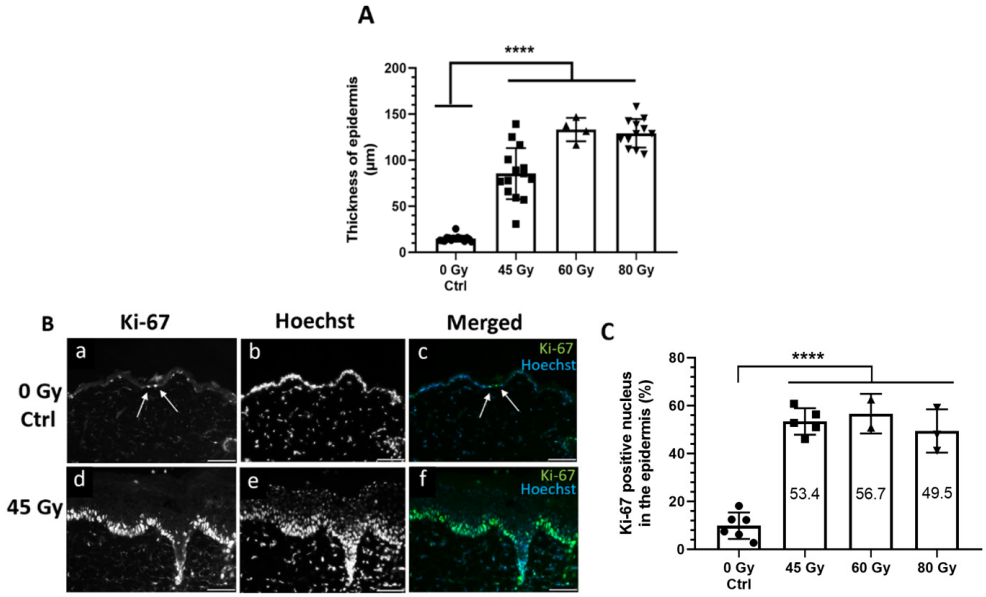

Figure 4. Epidermal thickness and Ki-67 expression are increased in murine irradiated epidermis 28 days after irradiation. (**A**) Mean thickness of the epidermal compartment. Statistics: mean ± SD. n = 4–16 mice/group. (**B**) Immunolabeling for Ki-67 on a representative skin biopsy 28 days after irradiation with a 45 Gy dose in comparison to normal skin. Nuclei are stained with Hoechst. Bars = 100 µm. (**C**) Quantification reveals a significant increase of Ki-67 positive nuclei in the epidermis of irradiated compared to non-irradiated skin. Statistics: mean ± SD. n = 2–6 mice/group, One-way ANOVA with Dunnett's multiple comparisons test **** $p < 0.0001$.

3.3. Evidence of Dermal Damage and dWAT Thinning 28 Days after Irradiation

Following histology processing and Masson's trichrome staining of skin samples, cells appear in pink, matrix elements of the dermis appear in blue, and the adipocytes of the dermal white adipose tissue (dWAT) appears as blank spaces (Figure 3). Measurements of the thickness of the dermal compartment showed a significant increase of 1.3-fold for the dose of 45 Gy, and 1.4-fold for the dose of 80 Gy in comparison to non-irradiation skin, while only a slight increase in dermal thickness was observed for the 60 Gy dose for which a smaller number of samples were available (n = 4 mice) (Figure 5A). In addition, the dermis appeared to be more compact and denser in irradiated than in normal skin (Figure 3). Immunofluorescence labeling directed against alpha-smooth muscle actin (α-

SMA), which is expressed by myofibroblasts, revealed a large number of these contractile cells in the irradiated tissue (Figure 5B). The quantification of positive α-SMA labeling per mm^2 in the papillary dermis of normal skin was 1.1 ± 0.3%, while irradiated skin showed a dose-dependent increase of 1.7-, 1.9-, and 2.4-fold for the 45, 60, and 80 Gy doses, respectively (Figure 5C). Finally, measurements of the thickness of the dWAT layer of irradiated skin revealed a decrease in thickness from 210.7 ± 125.2 µm in normal skin to mean values of 127.9 ± 53.8 µm, 190.9 ± 99.9 µm, and 117.2 ± 63.8 µm for the 45, 60, and 80 Gy doses, respectively ($p = 0.06$) (Figures 3 and 5D).

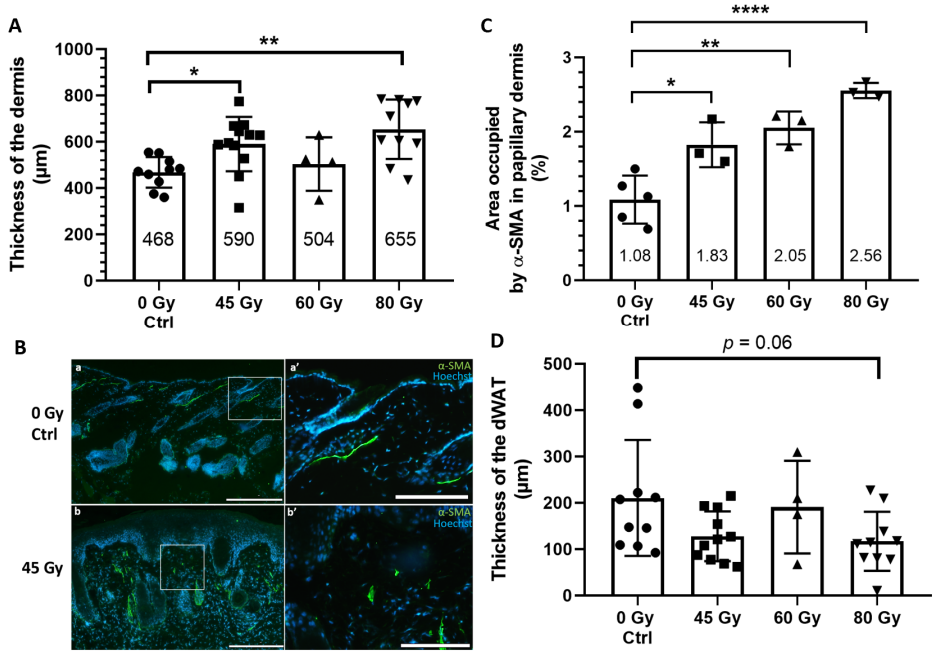

Figure 5. Impact on connective tissue compartments 28 days after irradiation. (**A**) Mean thickness of dermis. (**B**) Immunolabeling for α-SMA on (**a**) a representative skin biopsy of non-irradiated control skin and (**b**) 28 days after irradiation with a 45 Gy radiation dose. (**a'**,**b'**) are magnifications of the areas delimited by the white boxes in (**a**,**b**). Bars (**a**,**b**) = 500 µm; (**a'**,**b'**) = 200 µm. Nuclei were stained with Hoechst. (**C**) Quantification of α-SMA labeling associated with the presence of myofibroblasts in the papillary dermis 28 days after irradiation. (**D**) Mean thickness of the dermal white adipose tissue layer (dWAT). Statistics: mean ± SD. n = 3–16 mice/group, One-way ANOVA with Dunnett's multiple comparison tests * $p < 0.05$, ** $p < 0.01$, **** $p < 0.0001$.

3.4. Capillary Vessels Are Altered in Irradiated Skin

Twenty-eight days after irradiation, capillary vessel density was evaluated in normal as well as irradiated skin by the immunolabeling of CD31-expressing endothelial cells on transverse cryosections (Figure 6). A network of blood vessel structures was clearly visible within the dermis of normal skin (Figure 6Aa', 0 Gy magnification), while vessel presence was significantly reduced by almost twofold in 80 Gy irradiated skin (Figure 6A,B). Moreover, the morphology of the blood vessels appeared to be altered, with the presence of numerous fragmented structures (Figure 6Ab', 80 Gy magnification). Vascularity also tended to decrease in skin irradiated with the 45 Gy and 60 Gy doses.

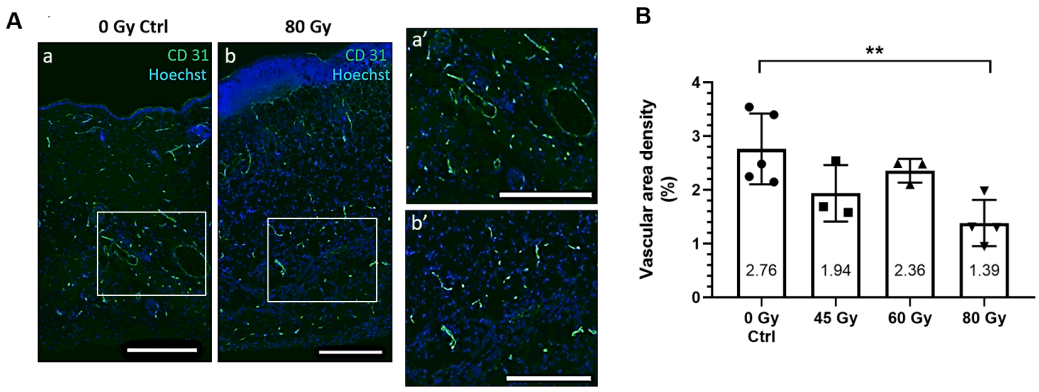

Figure 6. Vascularity is altered in irradiated skin. (**A**) Immunolabeling for CD31 on a representative skin section of (**a**) non-irradiated control skin, and (**b**) 80 Gy irradiated skin 28 days after irradiation. Nuclei are stained with Hoechst. (**a'**,**b'**) are magnifications of the areas delimited by the white boxes in (**a**,**b**). Bars = 200 µm. (**B**) Vascular area density determined from the quantification of CD31-positive structures present in the dermis. Statistics: mean ± SD. n = 3–5 mice/group, One-way ANOVA with Dunnett's multiple comparisons test ** $p < 0.01$.

3.5. Delayed Healing Kinetics of Excisional Wounds Created on Irradiated Skin in the Acute Stage of Radiodermatitis

In order to assess the kinetics and quality of the healing process mediated by skin cells during the earlier response phase after irradiation, full-thickness excision wounds were created in the center of the irradiated area (1 cm × 1 cm) four weeks after irradiation. The excisional wounds were smaller in diameter (8 mm) than the irradiated area, allowing the characterization of the healing properties of the cells originating from irradiated skin. A silicone-splinted model limiting the contraction associated with rodent skin was used. The overall appearance of the wounds was assessed from macroscopic images taken weekly (Figure 7A), and measurements of residual open wound areas over time were used to generate a mean percentage of wound closure (Figure 7B). Wounds created in irradiated skin showed a slower rate of healing, which was more evident from day 19 after surgery onwards. On day 33, the percentage of closure was lower for all irradiated groups, ranging from 69.9 ± 12.4% for the 45 Gy dose and 69.8 ± 8.4% for the 60 Gy dose in comparison to normal skin (87.0 ± 12.9%). The percentage of wound closure was significantly lower for the 80 Gy group which only achieved 56.8 ± 10.6% wound closure (Figure 7B).

Overall wound closure is an assessment that reflects the cumulative contributions of re-epithelialization, granulation tissue formation and putative residual wound contraction despite the use of a splinted model. Histological sections of Masson's trichrome-stained scar tissue representing the different doses revealed that during the 33 days of healing, complete wound re-epithelialization occurred for wounds in the control group, the 45 Gy group and most of the wounds of animals in the 60 Gy group. However, in the tissues of the 80 Gy group, some areas were devoid of neoepidermis, or when present, it consisted of only a few cell layers (Figure 8A, 80 Gy). For both higher doses, the granulation tissue appeared disorganized and was characterized by the presence of the underlying muscle emerging into the dermis (Figure 8A, red arrows). Moreover, the granulation tissue of mice from the 80 Gy group seemed hypocellular in some areas (Figure 8A, 80 Gy magnification). The content and distribution of the collagen fibers in the granulation tissue are better visualized after Picrosirius red staining (Figure 8B). Based on semi-quantitative analysis of the percentage of stained fibers, the collagen content in the granulation tissue of wounds created in normal skin was 1.7 to 2.3-fold more abundant than for those created in irradiated skin (Figure 8C).

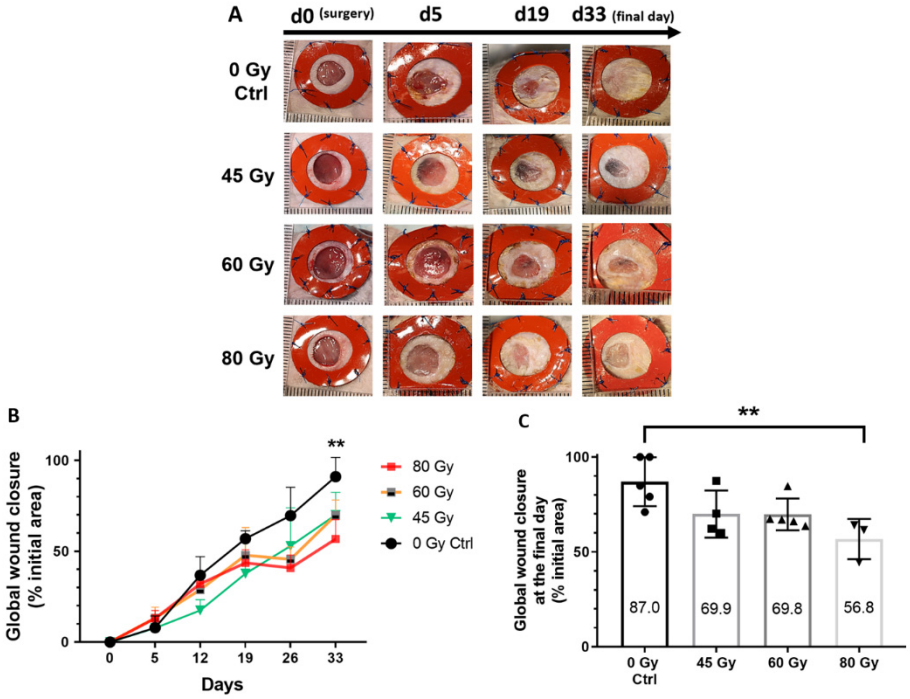

Figure 7. Healing kinetics of excisional wounds created on irradiated skin at the acute stage. (**A**) Macroscopic images showing the reduction in wound size over the course of 33 days after surgery. Measurements of global wound closure were made on such images for each wound, using ImageJ software. (**B**) Kinetics and (**C**) Global final wound closure values as a function of the dose received, reflecting the severity of the radiodermatitis that developed during four weeks prior to excisional surgery and splinting of the wounds. Statistics: mean ± SD. n = 3–5 mice/group, One-way ANOVA with Dunnett's multiple comparisons test ** $p < 0.01$. * Symbol indicates significance between control and other groups.

3.6. Healing of Incisional Wounds Created in Late Stages Irradiated Skin after Visual Resorption of Radiodermatitis

Next, we needed to determine if our in vivo model based on CD-1 mice could reproduce not only acute but also late cell responses to ionizing radiation indicative of chronic tissue damage. Indeed, patients receiving radiation therapy can develop acute (during and after radiotherapy sessions), and/or late tissue damage several weeks/months after the initial treatment. In our study, very few mice displayed recurrent redness of the lesions over several weeks (Table 1 and Figure 2). Most animals gradually progressed towards a macroscopic skin appearance reminiscent of healthy skin, namely, with the absence of notable scarring, and with the reappearance of hair follicles for all 45 and 60 Gy mice. As previously mentioned, the kinetics of radiodermatitis resorption differed according to the initial dose of ionizing radiation received (Figure 2), but ultimately lead to skin devoid of macroscopic features associated with radiation damage at the time chosen to perform a surgical challenge. At the histological level (Figure S2), the previously irradiated skin displayed a seemingly normal appearance for the 45 and 80 Gy groups, while the 60 Gy group still featured thickened epidermis and hair follicle outer root sheaths in some areas (Figure S2).

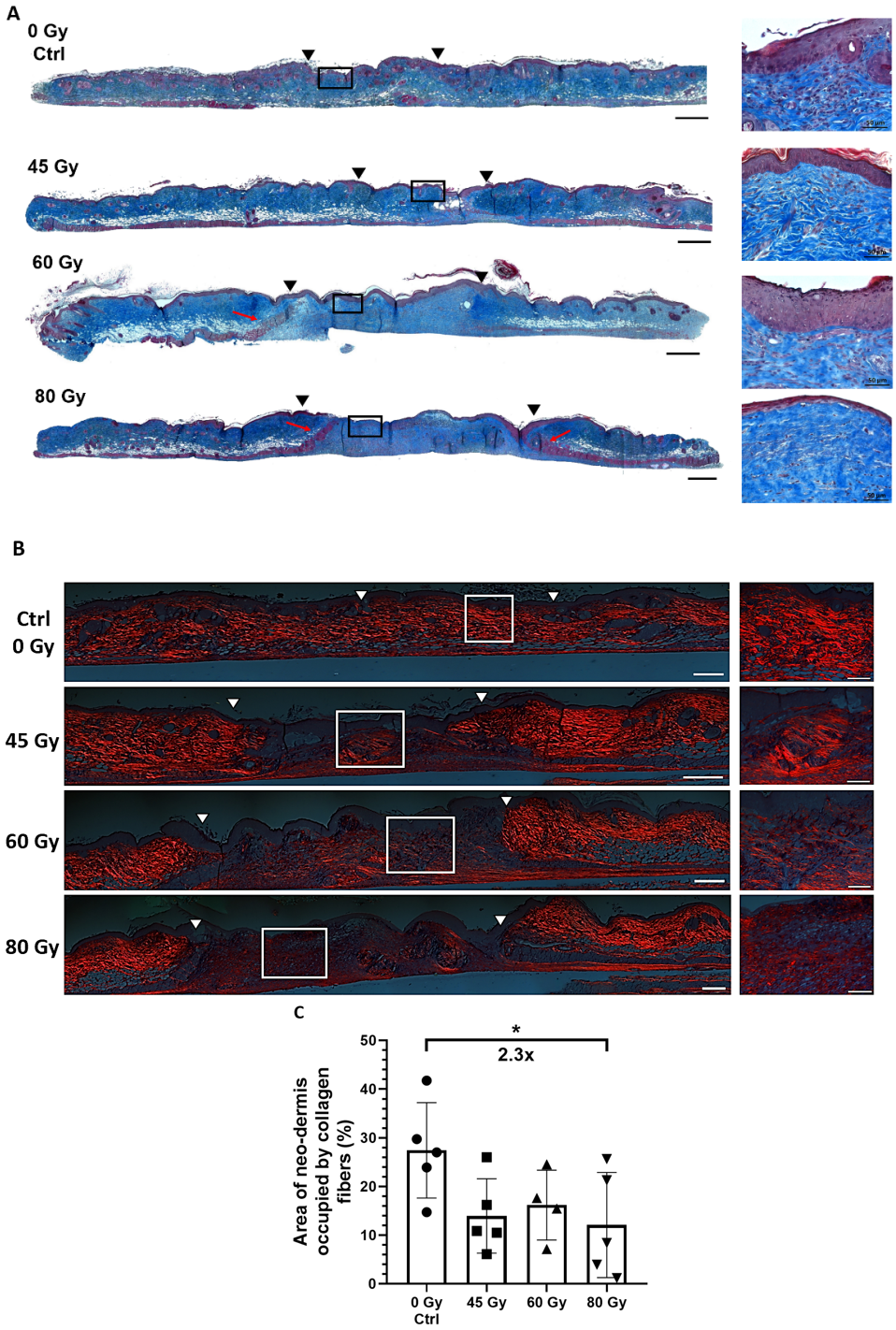

Figure 8. Appearance of the scar tissues after 33 days of healing. (**A**) Masson's trichrome staining of representative transverse sections of scar and adjacent tissues 33 days after excisional surgery performed on normal or irradiated skin. The margins corresponding to the site of the initial punch biopsy are indicated by arrowheads. Red arrows show the emergence of the underlying muscle into the dermis. Bars = 500 µm. Images on the right are magnifications of the corresponding boxed areas shown on the left. Bars = 50 µm. (**B**) Images of the wounds after Picrosirius red staining of contiguous paraffin-embedded tissue sections. Bars = 500 µm. Images on the right are magnifications of the corresponding boxed areas shown on the left. Bars = 50 µm. (**C**) Percentage of the granulation tissue area, identified by white arrowheads in B, occupied by collagen fibers. Statistics: mean ± SD. n = 4–5 mice/group, One-way ANOVA with Dunnett's multiple comparisons test * $p < 0.05$. * Symbol indicates significance between control and other groups.

An incisional wound model was chosen in order to reproduce the clinical situation where reconstructive surgery is needed after tumor ablation, but at a later time after radiotherapy treatments. For each group of irradiated animals, age-matched non-irradiated control mice also underwent surgery. The appearance of the incisions was documented by taking pictures of each wound every 2–3 days over 17 days, allowing the calculation of a mean healing score for four main outcomes (Table 2 and Figure 9A). The incisions made in non-irradiated skin quickly healed, with the scab falling off around day 10 post-surgery (Table 2). In comparison, the scab fell on day 13 (45 Gy), and days 15–16 (60 and 80 Gy) for irradiated skin. The final appearance of the scar was analyzed qualitatively on a scale of 0 to 3 (with 3 representing the most severe signs), according to the following criteria: redness/inflammation; contraction of the wound, and lack of cohesion of the wound margins (Table 2). On the 17th day after surgery (final day of analysis), the incisions made on normal skin showed complete healing without redness and with perfectly fused wound edges for all mice (100%). On average, these control mice were completely healed by the 15th day after surgery. For the incisions made in the irradiated skin, we observed impaired healing which increased in severity as a function of the radiation dose originally administered. Especially for the 80 Gy group, the incisions showed intense redness, more contraction and discontinuous union of the margins (Table 2 and Figure 9A). In summary, complete healing, as defined here by the absence of redness with a total union of the wound margins, was not observed for any irradiated group, proving that ionizing radiation caused deep and lasting skin damage even several weeks after the initial irradiation.

Table 2. Scoring of the appearance of the incisions indicating the severity of the healing complications.

		Healing Quality of the Scarring on the Final Day (Day 17)			
Dose (Gy) Number of Animals	**Shedding Time of Scabs**	**Redness Scoring/3**	**Contraction/Waviness Scoring/3**	**Non-Union of the Margins Scoring/3**	**Full Macroscopic Recovery (%)**
0 Gy Ctrl $n = 7$	Day 10	0/3	0.6/3	0/3	100% (Day 15)
45 Gy $n = 4$	Day 13	0.7/3	1.2/3	0.9/3	0%
60 Gy $n = 6$	Day 16	1.8/3	2.0/3	1.8/3	0%
80 Gy $n = 6$	Day 15	2.1/3	2.5/3	2.1/3	0%

3/3 high, 2/3 moderate, 1/3 low, 0/3 none.

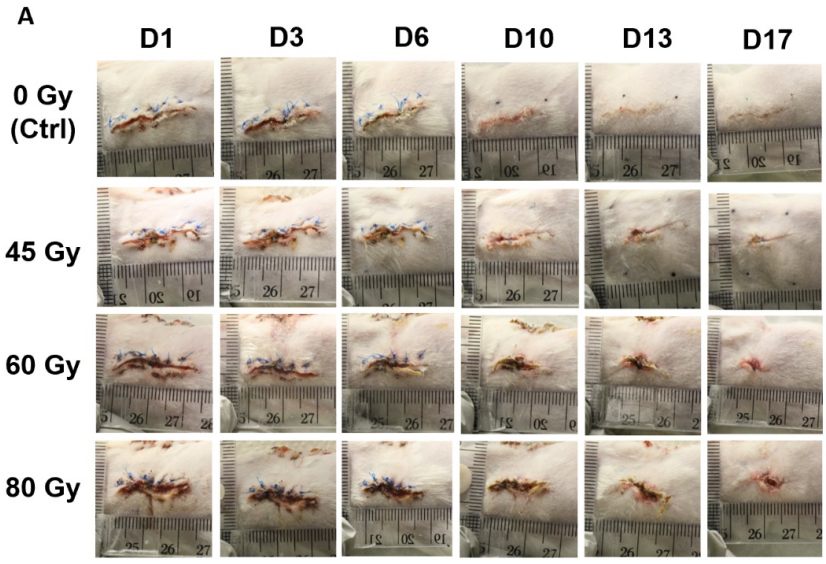

Figure 9. *Cont.*

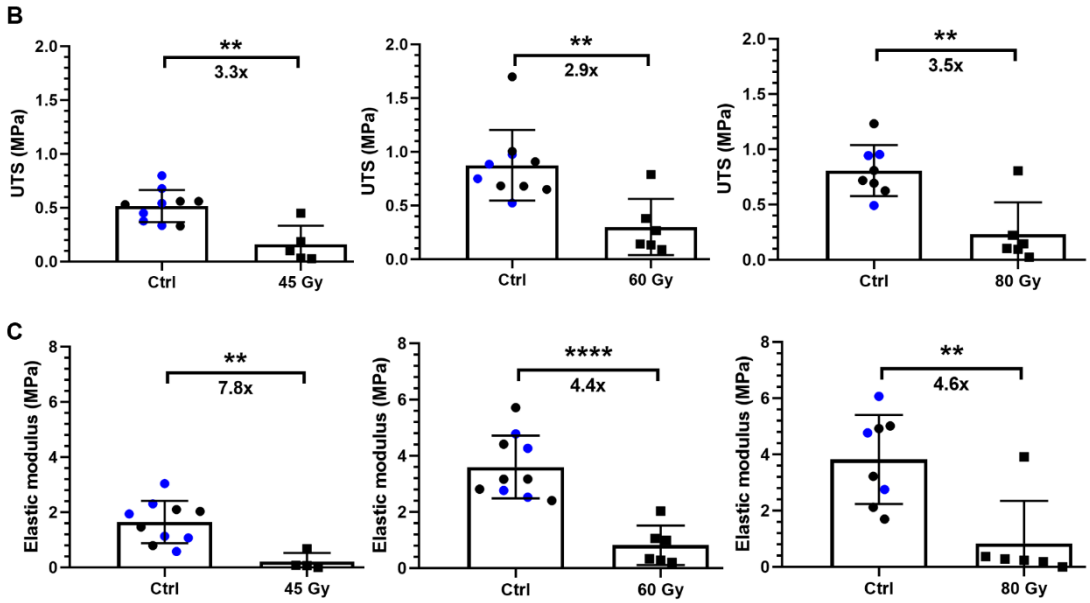

Figure 9. Healing kinetics of incisional wounds created on skin at late stages after irradiation. (**A**) Macroscopic images of the incisional wounds over the course of 17 days after surgery. (**B**,**C**) Mechanical test results performed 17 days after incisions were performed on normal or previously irradiated healed skin. (**B**) Ultimate tensile strength values. (**C**) Elastic modulus values. Data originating from the non-irradiated control mice are shown in dark blue in the graphs. Statistics: mean ± SD. n = 5–6 wounds for irradiated skin and n = 8–10 wounds for control skin. Unpaired t-tests ** $p < 0.01$, **** $p < 0.0001$.

In order to provide a quantitative and functional assessment of the incisional healing process, the mechanical properties of the scar tissues were evaluated 17 days after the initial surgery according to two parameters: the breaking strength and elasticity. Our results clearly show that scar tissue from incisions made in the irradiated skin had a significantly lower resistance to rupture than incisions made in the same anatomical region of non-irradiated mice of the same age (Figure 9B). Indeed, breaking force values for the 45 Gy-irradiated skin were reduced 3.3-fold, with UTS values of 0.16 ± 0.17 MPa compared to 0.52 ± 0.16 MPa for an incision made on normal skin. For the 60 and 80 Gy-irradiated skin, the mean breaking force values were reduced by 2.9 and 3.5-fold, respectively. These results indicate that scar tissue from incisions made in skin that received different radiation doses have recovery rates ranging from 3.0 to 8.9% of the original strength of intact non-wounded skin, while for non-irradiated normal skin, 9.8 to 26.1% of the original strength was regained 17 days after the incisions (Table 3). As for elasticity, scar tissue from incisions made in irradiated skin showed a significantly lower modulus of elasticity than incisions made in normal skin with values reduced by 7.8-, 4.4-, and 4.6-fold for the 45, 60, and 80 Gy groups, respectively (Figure 9C). This indicates that after 17 days of healing, incisions made in irradiated skin have a recovery rate ranging from 2.5 to 8.6% of the original elasticity of intact non-wounded skin, in comparison to recovery rates of 19.8 to 38.0% for the incisions made on normal skin depending on the age of the animals (Table 4).

Table 3. Ultimate tensile strength values for intact non-wounded skin compared with normal and irradiated skin incisions.

UTS Values for Intact Non-Wounded Age-Matched Murine Skin (MPa) (Age in Weeks) (Skin Thickness in μm)	Recovery for Normal Skin Incision (%) (Raw Values in MPa)	Recovery for Irradiated Skin Incision (%) (Raw Values in MPa)
5.31 ± 1.14 (22) (1.07 ± 0.09)	9.80% (0.52 ± 0.16)	45 Gy: 3.00% (0.16 ± 0.17)
3.37 ± 1.53 (36) (1.25 ± 0.13)	26.10% (0.88 ± 0.33)	60 Gy: 8.90% (0.30 ± 0.26)
4.04 ± 0.38 (27) (1.10 ± 0.07)	20.10% (0.81 ± 0.23)	80 Gy: 5.70% (0.23 ± 0.29)

Table 4. Modulus of elasticity values for intact non-wounded skin compared with normal and irradiated skin incisions.

Modulus of Elasticity for Intact Non-Wounded Age-Matched Murine Skin (MPa) (Age in Weeks) (Skin Thickness in μm)	Recovery for Normal Skin Incision (%) (Raw Values in MPa)	Recovery for Irradiated Skin Incision (%) (Raw Values in MPa)
8.35 ± 1.25 (22) (1.07 ± 0.09)	19.80% (1.65 ± 0.77)	45 Gy: 2.50% (0.21± 0.32)
9.51± 6.05 (36) (1.25 ± 0.13)	38.00% (3.61 ± 1.12)	60 Gy: 8.60% (0.82 ± 0.70)
11.29 ± 2.30 (27) (1.10 ± 0.07)	33.80% (3.82 ± 1.58)	80 Gy: 7.40% (0.83 ± 1.52)

4. Discussion

Radiodermatitis is a complex process that deeply affects the skin. Through the detailed characterization of a new murine model, our study shows the critical long-lasting impact of high doses of ionizing radiation on the three compartments of the skin (epidermis, dermis, and dWAT). The kinetics and severity of the impact of radiation were proportional to the dose of ionizing rays administered (single doses of 45, 60, or 80 Gy). The extended length of our post-radiation follow-up study (up to five months) provides important new results on irradiated skin physiopathology. Indeed, while some studies have focused on the long-term impact of single high doses of radiation on the mouse leg model [44] or hypofractionated radiation on the mouse ear model [45], we provide data on the impact of three single high radiation doses and associated healing of wounds created on the back of mice using a medical linear accelerator.

In the clinic, the incidence and the severity of radiodermatitis depends on the total dose received, the size of the irradiated zone and the design of fractionated dose regimens to help reduce chronic skin damage in cancer patients receiving radiotherapy [46]. We acknowledge that radiation delivered as a single dose is a limitation of many protocols using animal models, including ours, since it might induce greater skin damage than the fractionation schedule used for humans [46,47]. Nevertheless, our study used a medical

linear accelerator that provided a single dose of radiation over a small area (1 cm^2) precisely directed to the skin in order to recreate radiodermatitis features while minimizing the exposure of other organs to radiation. Interestingly, it has been reported that radiation doses twice as high as those inducing radiodermatitis symptoms in patients are required for rodents [32]. This is likely because of the very abundant hair follicles and glands of rodent skin, in addition to the size of the irradiation zone which is also smaller for animal studies [32].

Our study contributes new information documenting the radiosensitivity of CD-1 mice, a non-inbred line displaying higher inter-individual variability than inbred animals [48,49], and thus being more representative of the range of individual responses observed for patients [50]. Interestingly, we noticed a reactivation of radiodermatitis for some mice in the 45 and 60 Gy groups that were considered visually asymptomatic, a phenomenon also seen in humans. Skin repair and recovery from ionizing radiation for mice that received the 60 Gy dose was slow but continuous, reaching a total of 86% asymptomatic mice at day 155. In contrast, we observed that the high dose of 80 Gy induced scarring that did not significantly evolve 70 days after radiation, a sign of severe skin damage. This finding is in accordance with a recent study showing that in rats, a single dose of 90 Gy-irradiation to the leg showed a stalled evolution of the radiodermatitis from day 63 of healing until day 84, which corresponds to the final time-point of their study [51].

Our results show that at the earlier stage after irradiation at four weeks, the epidermis of the irradiated skin featured a hyperproliferative state. This is in agreement with the observations made on the skin of patients that developed early or late radiofibrosis symptoms after radiotherapy treatment [50]. The epidermis of patients has been described as hyperproliferative with a high level of Ki-67 positive cells from four weeks after irradiation [52]. Such hyperplastic epidermis was also associated with abnormal keratinocyte differentiation characterized by the expression of keratin (K) 6 and K16 in the suprabasal layers and a general disorganization of cytokeratins and involucrin at late stages after high doses of radiotherapy (up to 22 years after a total dose of 85 Gy) [53]. Few studies specifically investigated the impact of radiation on the epidermis [54,55] in comparison to the dermis for which the mechanisms driving radiofibrosis mediated by myofibroblasts are actively explored (reviewed in [12]). However, a recent study highlighted the role of IL-17 expressed by T lymphocytes in the mediation of inflammation and the hyperproliferation of keratinocytes following exposure to ionizing radiation [56]. The contribution of immune cells to radiodermatitis development and recurrence represents an interesting avenue of research, given the importance of immune cells (especially macrophages) in mediating wound chronicity [57,58].

In our study, we determined that the dermal thickness of irradiated skin was much greater than that of normal skin (1.4-fold, 80 Gy), with a strong presence of contractile myofibroblasts (α-SMA^+), of which the numbers increased with the radiation dose. This agrees with various preclinical and clinical studies that have documented the differentiation of fibroblasts into myofibroblasts under the action of TGF-β1, a major contributor to radiofibrosis (reviewed in [14]). DWAT is the deepest skin layer and its boundaries are not easily defined on histological sections. Our quantitative data indicates a trend towards a radiation-induced thinning of the dWAT layer. The latter may be related to the transdifferentiation of adipocytes into myofibroblasts, a process described in the fibrotic context of scleroderma [59,60]. Another recent study directly addressing the fate of adipocytes during the healing process has highlighted the role of adipose tissue in mediating inflammatory infiltration and the reprogramming of adipocytes into myofibroblasts [61]. We observed that four weeks after irradiation, skin vascularization was reduced by up to twofold compared with normal skin, depending on the dose. This could be due to apoptosis or altered endothelial cell function caused directly by ionizing radiation or by the presence of free radicals that are toxic to the cells [62–65]. It is recognized that irradiation profoundly affects the tissues by creating a hypoxic and pro-inflammatory environment detrimental to the proliferative phases of re-epithelialization and the formation of granulation tissue [12].

Next, we established that the skin alterations observed four weeks after radiation, namely a reduced vascularity and an increased fibrotic profile, translated into defective skin repair, not only at this early time-point, but also months later. By using two types of surgical challenge, a significant impairment of skin homeostasis was demonstrated, as late as 22 weeks after radiation. The wound repair data obtained following both excisional and incisional wounds on dorsal irradiated skin contribute complementary quantitative and functional evaluations indicating a significant and lasting skin damage by the ionizing rays. Our results indicate that the healing of full-thickness splinted excisional wounds created in irradiated skin is delayed by 20 to 35% depending on the dose, compared with normal skin wounds. Another team observed in rats a delay in healing of 8 mm diameter non-splinted excisional wounds created the same day that 10–40 Gy doses were delivered to the dorsal skin. Delayed healing was noted as early as day 14 post-surgery in their study, and the percentage of closure at day 21 (final day) was 37% for the 40 Gy group while the control group was totally healed at that time [66]. Other studies investigating potential wound treatment of irradiated skin observed a slight delayed contraction of non-splinted full-thickness wounds created immediately in 6 Gy irradiated skin versus normal skin [26,27]. Finally, our histological analyses of the scar tissue of irradiated skin support a delay in wound reepithelization created in 80 Gy irradiated skin, associated with hypocellularity, disorganization and a decrease in collagen fibers (2.3-fold, 80 Gy) in the granulation tissue.

While the study of large full-thickness splinted excisional wounds allows more quantitative follow-up and is, to some extent, representative of the context of cancer tumor resection or reconstructive surgery after radiotherapy [31], an incisional wound model is the most appropriate for assessing the mechanical properties of scar tissue [67]. The thickness and mechanical properties of murine skin differ according to the age and weight of the mouse, so it is critical to compare mechanical values between mice of the same age [68–70]. In our study, we observed that the resistance to rupture was reduced by more than 66% after 17 days of healing for the incision made on 60 Gy-irradiated skin compared to an incision made on normal skin. Our data are in agreement with other studies which observed that the resistance to rupture of the wound created in guinea pig skin was reduced by 62% of the value for normal skin in skin irradiated at 18 Gy compared to an incision made in normal skin after seven days of healing [21]. In another study in mice, the resistance to wound rupture was reduced by 70% of normal values for skin irradiated with 18 Gy after 14 days of healing [22]. Such scar rupture values suggest that the deposition of collagen fibers is still immature in the granulation tissue of irradiated skin [25,71]. As for the modulus of elasticity, it was reduced by more than 77% for incisions made on 60 and 80 Gy- irradiated skin compared with an incision made on normal skin, suggesting that the scar tissue of the irradiated skin lacks rigidity, which may also be a sign of altered remodeling of the extracellular matrix. It has been previously shown that irradiation reduces the rigidity of collagen scaffolding in vitro and disrupts the primary helical collagen structure [72]. Combined with studies reporting that irradiation impacts the level of metalloproteinases, this could explain the resulting altered matrix remodeling observed [66,73]. To our knowledge, among the few studies using an incision wound model on irradiated skin [22,23,25], our data are the first report of the outcomes of incisional wounding on macroscopically healed irradiated skin at very late stages (up to 22 weeks) after the initial irradiation. This is reminiscent of the clinical context, as it is strongly recommended to perform reconstructive surgery several weeks after the last radiotherapy session whenever possible [74].

5. Conclusions

Globally, these results show our ability to recreate moderate to more severe grade radiodermatitis of the skin based on three single high radiation doses. This study provides important new data documenting the progression of radiodermatitis symptoms at early and late stages after radiation. The latter causes significant tissue damage resulting in fibrotic and poorly vascularized tissue unable to support proper healing. The functional

mechanical properties of the skin after exposure to ionizing radiation are also profoundly affected. This increased understanding of radiation damage to the skin and the validation of our murine model for studying the development of severe radiodermatitis will guide studies aimed at evaluating the effectiveness of various treatment modalities with the goal of significantly improving the management this type of incapacitating difficult-to-heal wound.

Supplementary Materials: The following are available online at https://www.mdpi.com/2017-2017/2/1/4/s1.

Author Contributions: Conceptualization, C.D., J.F., and L.A.; methodology, C.D., C.J.H., M.S., C.P., J.G., J.L., and L.A.; validation, J.R., L.A., J.G., and J.L.; formal analysis, C.D., C.J.H., and J.F.; resources, J.F., L.A., and J.R.; data curation, C.D. and J.F.; writing—original draft preparation, C.D. and J.F.; writing—review and editing, C.D., C.J.H., J.F., J.L., J.R., L.A., M.S., and V.T.; supervision, J.F.; project administration, J.F.; funding acquisition, J.F. and L.A.; All authors have read and agreed to the published version of the manuscript.

Funding: This research was funded by the Canadian Institutes of Health Research (CIHR), Institute of Musculoskeletal Health and Arthritis catalyst Grant # 384224/151708, as well as internal grants from the regenerative medicine axis of the Centre de recherche du CHU de Québec-Université Laval (CRCHU), a Fonds de recherche du Québec–Santé (FRQS) funded Research Center, and the Fondation du CHU de Québec-Université Laval. We acknowledge the support of the Québec Cell, Tissue and Gene Therapy Network–ThéCell (a thematic network supported by the FRQS). C.D is grateful for the graduate studies scholarships "Joseph Demers" from Université Laval Faculty of Medicine, from he Fondation du CHU de Québec-U. Laval, from the LOEX and from le Fonds de la recherche du Québec–Nature et Technologies (FRQNT).

Institutional Review Board Statement: For studies involving animals, protocols (#17-051, 18 July, 2019) were approved by the Comité de Protection des Animaux de l'Université Laval (CPAUL) and Cégep de Sainte-Foy Animal Protection Committees.

Informed Consent Statement: Not applicable.

Data Availability Statement: The data supporting the findings presented in this study are available on request from the corresponding author.

Acknowledgments: The authors would like to acknowledge the valuable contribution of Dominique Mayrand, Marc-André Plourde-Campagna, the histology team members, as well as the animal facility technicians of Hôpital de l'Enfant-Jésus, more specifically Karine Pichette, Emilie Méthot-Lauzé, Sabrina Béland and Sabrina Dick. We would like to thank the Cégep Sainte-Foy, the Centre de recherche du CHU de Québec-Université Laval (CRCHU), as well as the histology platform of the CRCHU.

Conflicts of Interest: The authors declare no conflict of interest.

References

1. Delaney, G.; Jacob, S.; Featherstone, C.; Barton, M. The role of radiotherapy in cancer treatment: Estimating optimal utilization from a review of evidence-based clinical guidelines. *Cancer* **2005**, *104*, 1129–1137. [CrossRef] [PubMed]
2. Baskar, R.; Lee, K.A.; Yeo, R.; Yeoh, K.W. Cancer and radiation therapy: Current advances and future directions. *Int. J. Med. Sci.* **2012**, *9*, 193–199. [CrossRef] [PubMed]
3. Maddocks-Jennings, W.; Wilkinson, J.M.; Shillington, D. Novel approaches to radiotherapy-induced skin reactions: A literature review. *Complement. Ther. Clin. Pr.* **2005**, *11*, 224–231. [CrossRef] [PubMed]
4. McQuestion, M. Evidence-based skin care management in radiation therapy: Clinical update. *Semin. Oncol. Nurs.* **2011**, *27*, e1–e17. [CrossRef]
5. Salvo, N.; Barnes, E.; van Draanen, J.; Stacey, E.; Mitera, G.; Breen, D.; Giotis, A.; Czarnota, G.; Pang, J.; De Angelis, C. Prophylaxis and management of acute radiation-induced skin reactions: A systematic review of the literature. *Curr. Oncol.* **2010**, *17*, 94–112.
6. Singh, M.; Alavi, A.; Wong, R.; Akita, S. Radiodermatitis: A Review of Our Current Understanding. *Am. J. Clin. Dermatol.* **2016**, *17*, 277–292. [CrossRef]
7. Mendelsohn, F.A.; Divino, C.M.; Reis, E.D.; Kerstein, M.D. Wound care after radiation therapy. *Adv. Ski. Wound Care* **2002**, *15*, 216–224. [CrossRef]
8. Brown, K.R.; Rzucidlo, E. Acute and chronic radiation injury. *J. Vasc. Surg.* **2011**, *53*, 15S–21S. [CrossRef]

9. Lataillade, J.J.; Doucet, C.; Bey, E.; Carsin, H.; Huet, C.; Clairand, I.; Bottollier-Depois, J.F.; Chapel, A.; Ernou, I.; Gourven, M.; et al. New approach to radiation burn treatment by dosimetry-guided surgery combined with autologous mesenchymal stem cell therapy. *Regen. Med.* **2007**, *2*, 785–794. [CrossRef]
10. Bey, E.; Duhamel, P.; Lataillade, J.J.; de Revel, T.; Carsin, H.; Gourmelon, P. Treatment of radiation burns with surgery and cell therapy. A report of two cases. *Bull. Acad. Natl. Med.* **2007**, *191*, 971–978, discussion 979.
11. Ryan, J.L. Ionizing radiation: The good, the bad, and the ugly. *J. Investig. Dermatol.* **2012**, *132*, 985–993. [CrossRef] [PubMed]
12. Ejaz, A.; Greenberger, J.S.; Rubin, P.J. Understanding the mechanism of radiation induced fibrosis and therapy options. *Pharmacol. Ther.* **2019**, *204*, 107399. [CrossRef] [PubMed]
13. Ejaz, A.; Epperly, M.W.; Hou, W.; Greenberger, J.S.; Rubin, J.P. Adipose-Derived Stem Cell Therapy Ameliorates Ionizing Irradiation Fibrosis via Hepatocyte Growth Factor-Mediated Transforming Growth Factor-beta Downregulation and Recruitment of Bone Marrow Cells. *Stem Cells* **2019**, *37*, 791–802. [CrossRef]
14. Martin, M.; Lefaix, J.; Delanian, S. TGF-beta1 and radiation fibrosis: A master switch and a specific therapeutic target? *Int. J. Radiat. Oncol. Biol. Phys.* **2000**, *47*, 277–290. [CrossRef]
15. Milliat, F.; Francois, A.; Isoir, M.; Deutsch, E.; Tamarat, R.; Tarlet, G.; Atfi, A.; Validire, P.; Bourhis, J.; Sabourin, J.C.; et al. Influence of endothelial cells on vascular smooth muscle cells phenotype after irradiation: Implication in radiation-induced vascular damages. *Am. J. Pathol.* **2006**, *169*, 1484–1495. [CrossRef] [PubMed]
16. Davis, A.M.; O'Sullivan, B.; Turcotte, R.; Bell, R.; Catton, C.; Chabot, P.; Wunder, J.; Hammond, A.; Benk, V.; Kandel, R.; et al. Late radiation morbidity following randomization to preoperative versus postoperative radiotherapy in extremity soft tissue sarcoma. *Radiother. Oncol.* **2005**, *75*, 48–53. [CrossRef] [PubMed]
17. O'Sullivan, B.; Davis, A.M.; Turcotte, R.; Bell, R.; Catton, C.; Chabot, P.; Wunder, J.; Kandel, R.; Goddard, K.; Sadura, A.; et al. Preoperative versus postoperative radiotherapy in soft-tissue sarcoma of the limbs: A randomised trial. *Lancet* **2002**, *359*, 2235–2241. [CrossRef]
18. Tumerdem-Ulug, B.; Kuran, I.; Ozden, B.C.; Mete, O.; Kemikler, G.; Aktas, S.; Calik, B. Does hyperbaric oxygen administration before or after irradiation decrease side effects of irradiation on implant sites? *Ann. Plast. Surg.* **2011**, *67*, 62–67. [CrossRef]
19. Vandeweyer, E.; Deraemaecker, R. Radiation therapy after immediate breast reconstruction with implants. *Plast. Reconstr. Surg.* **2000**, *106*, 56–58, discussion 59–60. [CrossRef]
20. Forman, D.L.; Chiu, J.; Restifo, R.J.; Ward, B.A.; Haffty, B.; Ariyan, S. Breast reconstruction in previously irradiated patients using tissue expanders and implants: A potentially unfavorable result. *Ann. Plast. Surg.* **1998**, *40*, 360–363, discussion 363–364. [CrossRef]
21. Bernstein, E.F.; Salomon, G.D.; Harisiadis, L.; Talbot, T.; Harrington, F.; Russo, A.; Uitto, J. Collagen gene expression and wound strength in normal and radiation-impaired wounds. A model of radiation-impaired wound healing. *J. Dermatol. Surg. Oncol.* **1993**, *19*, 564–570. [CrossRef] [PubMed]
22. Gorodetsky, R.; McBride, W.H.; Withers, H.R. Assay of radiation effects in mouse skin as expressed in wound healing. *Radiat. Res.* **1988**, *116*, 135–144. [CrossRef] [PubMed]
23. Mustoe, T.A.; Pierce, G.F.; Thomason, A.; Gramates, P.; Sporn, M.B.; Deuel, T.F. Accelerated healing of incisional wounds in rats induced by transforming growth factor-beta. *Science* **1987**, *237*, 1333–1336. [CrossRef] [PubMed]
24. Mustoe, T.A.; Purdy, J.; Gramates, P.; Deuel, T.F.; Thomason, A.; Pierce, G.F. Reversal of impaired wound healing in irradiated rats by platelet-derived growth factor-BB. *Am. J. Surg.* **1989**, *158*, 345–350. [CrossRef]
25. Tibbs, M.K. Wound healing following radiation therapy: A review. *Radiother. Oncol.* **1997**, *42*, 99–106. [CrossRef]
26. Jagetia, G.C.; Rajanikant, G.K. Effect of curcumin on radiation-impaired healing of excisional wounds in mice. *J. Wound Care* **2004**, *13*, 107–109. [CrossRef]
27. El-Hamoly, T.; El-Denshary, E.S.; Saad, S.M.; El-Ghazaly, M.A. 3-aminobenzamide, a poly (ADP ribose) polymerase inhibitor, enhances wound healing in whole body gamma irradiated model. *Wound Repair Regen.* **2015**, *23*, 672–684. [CrossRef]
28. Galiano, R.D.; Michaels, J.T.; Dobryansky, M.; Levine, J.P.; Gurtner, G.C. Quantitative and reproducible murine model of excisional wound healing. *Wound Repair Regen.* **2004**, *12*, 485–492. [CrossRef]
29. Morissette Martin, P.; Maux, A.; Laterreur, V.; Mayrand, D.; Gagné, V.L.; Moulin, V.J.; Fradette, J. Enhancing repair of full-thickness excisional wounds in a murine model: Impact of tissue-engineered biological dressings featuring human differentiated adipocytes. *Acta Biomater.* **2015**, *22*, 39–49. [CrossRef]
30. Michaels, J.T.; Churgin, S.S.; Blechman, K.M.; Greives, M.R.; Aarabi, S.; Galiano, R.D.; Gurtner, G.C. db/db mice exhibit severe wound-healing impairments compared with other murine diabetic strains in a silicone-splinted excisional wound model. *Wound Repair Regen.* **2007**, *15*, 665–670. [CrossRef]
31. Werier, J.; Ferguson, P.; Bell, R.; Hill, R.; Wunder, J.; O'Sullivan, B.; Kandel, R. Model of radiation-impaired healing of a deep excisional wound. *Wound Repair Regen.* **2006**, *14*, 498–505. [CrossRef] [PubMed]
32. Williams, J.P.; Brown, S.L.; Georges, G.E.; Hauer-Jensen, M.; Hill, R.P.; Huser, A.K.; Kirsch, D.G.; Macvittie, T.J.; Mason, K.A.; Medhora, M.M.; et al. Animal models for medical countermeasures to radiation exposure. *Radiat. Res.* **2010**, *173*, 557–578. [CrossRef] [PubMed]
33. Hegedus, F.; Mathew, L.M.; Schwartz, R.A. Radiation dermatitis: An overview. *Int. J. Dermatol.* **2017**, *56*, 909–914. [CrossRef] [PubMed]

34. Chan, R.J.; Webster, J.; Chung, B.; Marquart, L.; Ahmed, M.; Garantziotis, S. Prevention and treatment of acute radiation-induced skin reactions: A systematic review and meta-analysis of randomized controlled trials. *BMC Cancer* **2014**, *14*, 53. [CrossRef]
35. Iacovelli, N.A.; Galaverni, M.; Cavallo, A.; Naimo, S.; Facchinetti, N.; Iotti, C.; Fallai, C.; Orlandi, E. Prevention and treatment of radiation-induced acute dermatitis in head and neck cancer patients: A systematic review. *Future Oncol.* **2018**, *14*, 291–305. [CrossRef]
36. Lin, L.C.; Que, J.; Lin, L.K.; Lin, F.C. Zinc supplementation to improve mucositis and dermatitis in patients after radiotherapy for head-and-neck cancers: A double-blind, randomized study. *Int. J. Radiat. Oncol. Biol. Phys.* **2006**, *65*, 745–750. [CrossRef]
37. Vadarli, G.; Angelo-Khattar, M. A Fibroblast-Derived Human Growth Factor Preparation for the Management of Acute Radiodermatitis: A Case Report. *Int. Med. Case Rep. J.* **2020**, *13*, 691–696. [CrossRef]
38. Landry, Y.; Le, O.; Mace, K.A.; Restivo, T.E.; Beausejour, C.M. Secretion of SDF-1alpha by bone marrow-derived stromal cells enhances skin wound healing of C57BL/6 mice exposed to ionizing radiation. *J. Cell. Mol. Med.* **2010**, *14*, 1594–1604. [CrossRef]
39. Huang, S.P.; Huang, C.H.; Shyu, J.F.; Lee, H.S.; Chen, S.G.; Chan, J.Y.; Huang, S.M. Promotion of wound healing using adipose-derived stem cells in radiation ulcer of a rat model. *J. Biomed. Sci.* **2013**, *20*, 51. [CrossRef]
40. Kim, W.S.; Park, B.S.; Sung, J.H.; Yang, J.M.; Park, S.B.; Kwak, S.J.; Park, J.S. Wound healing effect of adipose-derived stem cells: A critical role of secretory factors on human dermal fibroblasts. *J. Dermatol. Sci.* **2007**, *48*, 15–24. [CrossRef]
41. Rehman, J.; Traktuev, D.; Li, J.; Merfeld-Clauss, S.; Temm-Grove, C.J.; Bovenkerk, J.E.; Pell, C.L.; Johnstone, B.H.; Considine, R.V.; March, K.L. Secretion of angiogenic and antiapoptotic factors by human adipose stromal cells. *Circulation* **2004**, *109*, 1292–1298. [CrossRef] [PubMed]
42. Chamberlain, G.; Fox, J.; Ashton, B.; Middleton, J. Concise review: Mesenchymal stem cells: Their phenotype, differentiation capacity, immunological features, and potential for homing. *Stem Cells* **2007**, *25*, 2739–2749. [CrossRef] [PubMed]
43. Junqueira, L.C.; Bignolas, G.; Brentani, R.R. Picrosirius staining plus polarization microscopy, a specific method for collagen detection in tissue sections. *Histochem. J.* **1979**, *11*, 447–455. [CrossRef] [PubMed]
44. Classen, J.; Paulsen, F.; Hehr, T.; Bamberg, M.; Budach, W. Effect of gemcitabine on acute and late radiation toxicity of skin and underlying soft tissues to single-dose irradiation in a nude mice model. *Int. J. Radiat. Oncol. Biol. Phys.* **2002**, *53*, 197–205. [CrossRef]
45. Dombrowsky, A.C.; Schauer, J.; Sammer, M.; Blutke, A.; Walsh, D.W.M.; Schwarz, B.; Bartzsch, S.; Feuchtinger, A.; Reindl, J.; Combs, S.E.; et al. Acute Skin Damage and Late Radiation-Induced Fibrosis and Inflammation in Murine Ears after High-Dose Irradiation. *Cancers* **2019**, *11*, 727. [CrossRef] [PubMed]
46. Thames, H.D., Jr.; Withers, H.R.; Peters, L.J.; Fletcher, G.H. Changes in early and late radiation responses with altered dose fractionation: Implications for dose-survival relationships. *Int. J. Radiat. Oncol. Biol. Phys.* **1982**, *8*, 219–226. [CrossRef]
47. Cosset, J.M.; Mornex, F.; Eschwege, F. Hypofractionation and radiotherapy: "The eternal return". *Cancer Radiother.* **2013**, *17*, 355–362. [CrossRef] [PubMed]
48. Aldinger, K.A.; Sokoloff, G.; Rosenberg, D.M.; Palmer, A.A.; Millen, K.J. Genetic variation and population substructure in outbred CD-1 mice: Implications for genome-wide association studies. *PLoS ONE* **2009**, *4*, e4729. [CrossRef] [PubMed]
49. Festing, M.F. Evidence should trump intuition by preferring inbred strains to outbred stocks in preclinical research. *ILAR J.* **2014**, *55*, 399–404. [CrossRef] [PubMed]
50. Hymes, S.R.; Strom, E.A.; Fife, C. Radiation dermatitis: Clinical presentation, pathophysiology, and treatment 2006. *J. Am. Acad. Dermatol.* **2006**, *54*, 28–46. [CrossRef] [PubMed]
51. Sheng, X.; Zhou, Y.; Wang, H.; Shen, Y.; Liao, Q.; Rao, Z.; Deng, F.; Xie, L.; Yao, C.; Mao, H.; et al. Establishment and characterization of a radiation-induced dermatitis rat model. *J. Cell. Mol. Med.* **2019**, *23*, 3178–3189. [CrossRef] [PubMed]
52. Joiner, M.C.; Marples, B.; Lambin, P.; Short, S.C.; Turesson, I. Low-dose hypersensitivity: Current status and possible mechanisms. *Int. J. Radiat. Oncol. Biol. Phys.* **2001**, *49*, 379–389. [CrossRef]
53. Sivan, V.; Vozenin-Brotons, M.C.; Tricaud, Y.; Lefaix, J.L.; Cosset, J.M.; Dubray, B.; Martin, M.T. Altered proliferation and differentiation of human epidermis in cases of skin fibrosis after radiotherapy. *Int. J. Radiat. Oncol. Biol. Phys.* **2002**, *53*, 385–393. [CrossRef]
54. Liu, K.; Kasper, M.; Trott, K.R. Changes in keratinocyte differentiation during accelerated repopulation of the irradiated mouse epidermis. *Int. J. Radiat. Biol.* **1996**, *69*, 763–769. [CrossRef] [PubMed]
55. Turesson, I.; Nyman, J.; Qvarnstrom, F.; Simonsson, M.; Book, M.; Hermansson, I.; Sigurdardottir, S.; Johansson, K.A. A low-dose hypersensitive keratinocyte loss in response to fractionated radiotherapy is associated with growth arrest and apoptosis. *Radiother. Oncol.* **2010**, *94*, 90–101. [CrossRef] [PubMed]
56. Liao, W.; Hei, T.K.; Cheng, S.K. Radiation-Induced Dermatitis is Mediated by IL17-Expressing gammadelta T Cells. *Radiat. Res.* **2017**, *187*, 454–464. [CrossRef] [PubMed]
57. Koh, T.J.; DiPietro, L.A. Inflammation and wound healing: The role of the macrophage. *Expert Rev. Mol. Med.* **2011**, *13*, e23. [CrossRef] [PubMed]
58. Wynn, T.A.; Vannella, K.M. Macrophages in Tissue Repair, Regeneration, and Fibrosis. *Immunity* **2016**, *44*, 450–462. [CrossRef] [PubMed]
59. Marangoni, R.G.; Lu, T.T. The roles of dermal white adipose tissue loss in scleroderma skin fibrosis. *Curr. Opin. Rheumatol.* **2017**, *29*, 585–590. [CrossRef]

60. Marangoni, R.G.; Korman, B.D.; Wei, J.; Wood, T.A.; Graham, L.V.; Whitfield, M.L.; Scherer, P.E.; Tourtellotte, W.G.; Varga, J. Myofibroblasts in murine cutaneous fibrosis originate from adiponectin-positive intradermal progenitors. *Arthritis Rheumatol.* **2015**, *67*, 1062–1073. [CrossRef] [PubMed]
61. Shook, B.A.; Wasko, R.R.; Mano, O.; Rutenberg-Schoenberg, M.; Rudolph, M.C.; Zirak, B.; Rivera-Gonzalez, G.C.; Lopez-Giraldez, F.; Zarini, S.; Rezza, A.; et al. Dermal Adipocyte Lipolysis and Myofibroblast Conversion Are Required for Efficient Skin Repair. *Cell Stem Cell* **2020**, *26*, 880–895.e6. [CrossRef] [PubMed]
62. Sugihara, T.; Hattori, Y.; Yamamoto, Y.; Qi, F.; Ichikawa, R.; Sato, A.; Liu, M.Y.; Abe, K.; Kanno, M. Preferential impairment of nitric oxide-mediated endothelium-dependent relaxation in human cervical arteries after irradiation. *Circulation* **1999**, *100*, 635–641. [CrossRef] [PubMed]
63. Venkatesulu, B.P.; Mahadevan, L.S.; Aliru, M.L.; Yang, X.; Bodd, M.H.; Singh, P.K.; Yusuf, S.W.; Abe, J.I.; Krishnan, S. Radiation-Induced Endothelial Vascular Injury: A Review of Possible Mechanisms. *JACC Basic Transl. Sci.* **2018**, *3*, 563–572. [CrossRef] [PubMed]
64. Langley, R.E.; Bump, E.A.; Quartuccio, S.G.; Medeiros, D.; Braunhut, S.J. Radiation-induced apoptosis in microvascular endothelial cells. *Br. J. Cancer* **1997**, *75*, 666–672. [CrossRef] [PubMed]
65. Gabrys, D.; Greco, O.; Patel, G.; Prise, K.M.; Tozer, G.M.; Kanthou, C. Radiation effects on the cytoskeleton of endothelial cells and endothelial monolayer permeability. *Int. J. Radiat. Oncol. Biol. Phys.* **2007**, *69*, 1553–1562. [CrossRef]
66. Jourdan, M.M.; Lopez, A.; Olasz, E.B.; Duncan, N.E.; Demara, M.; Kittipongdaja, W.; Fish, B.L.; Mader, M.; Schock, A.; Morrow, N.V.; et al. Laminin 332 deposition is diminished in irradiated skin in an animal model of combined radiation and wound skin injury. *Radiat. Res.* **2011**, *176*, 636–648. [CrossRef]
67. Madden, J.W.; Peacock, E.E., Jr. Studies on the biology of collagen during wound healing. I. Rate of collagen synthesis and deposition in cutaneous wounds of the rat. *Surgery* **1968**, *64*, 288–294.
68. Zomer, H.D.; Trentin, A.G. Skin wound healing in humans and mice: Challenges in translational research. *J. Dermatol. Sci.* **2018**, *90*, 3–12. [CrossRef]
69. Lynch, B.; Bonod-Bidaud, C.; Ducourthial, G.; Affagard, J.S.; Bancelin, S.; Psilodimitrakopoulos, S.; Ruggiero, F.; Allain, J.M.; Schanne-Klein, M.C. How aging impacts skin biomechanics: A multiscale study in mice. *Sci. Rep.* **2017**, *7*, 13750. [CrossRef]
70. Reiser, K.M. Influence of age and long-term dietary restriction on enzymatically mediated crosslinks and nonenzymatic glycation of collagen in mice. *J. Gerontol.* **1994**, *49*, B71–B79. [CrossRef]
71. Delanian, S.; Martin, M.; Bravard, A.; Luccioni, C.; Lefaix, J.L. Abnormal phenotype of cultured fibroblasts in human skin with chronic radiotherapy damage. *Radiother. Oncol.* **1998**, *47*, 255–261. [CrossRef]
72. Miller, J.P.; Borde, B.H.; Bordeleau, F.; Zanotelli, M.R.; LaValley, D.J.; Parker, D.J.; Bonassar, L.J.; Pannullo, S.C.; Reinhart-King, C.A. Clinical doses of radiation reduce collagen matrix stiffness. *APL Bioeng.* **2018**, *2*, 031901. [CrossRef] [PubMed]
73. Gu, Q.; Wang, D.; Gao, Y.; Zhou, J.; Peng, R.; Cui, Y.; Xia, G.; Qing, Q.; Yang, H.; Liu, J.; et al. Expression of MMP1 in surgical and radiation-impaired wound healing and its effects on the healing process. *J. Environ. Pathol. Toxicol. Oncol.* **2002**, *21*, 71–78. [CrossRef] [PubMed]
74. Dewael, S.; Vandevoort, M.; Fabre, G.; Nanhekhan, L. Immediate versus delayed autologous breast reconstruction: A retrospective matched cohort study of irradiated patients. *J. Plast. Reconstr. Aesthet. Surg.* **2019**, *72*, 1769–1775. [CrossRef]